ISSN 1070-3284, Russian Journal of Coordination Chemistry, 2022, Vol. 48, No. 7, pp. 436–451. © Pleiades Publishing, Ltd., 2022.
Russian Text © The Author(s), 2022, published in Koordinatsionnaya Khimiya, 2022, Vol. 48, No. 7, pp. 428–444.

The authors congratulate Academician V.I. Ovcharenko on the occasion of his 70th jubilee

Rare-Earth Metal (Pr(III), Tb(III), Ho(III), and Er(III)) Complexes with 2-Mercaptopyridine-*N*-oxide: Synthesis, Structures, and Properties

V. P. Shtefanets[a], G. V. Shilov[b], E. I. Kunitsyna[b], R. B. Morgunov[b], N. A. Sanina[b, *], and S. M. Aldoshin[b]

[a] *Moscow Institute of Physics and Technology (National Research University), Dolgoprudnyi, Moscow oblast, Russia*

[b] *Institute of Problems of Chemical Physics, Russian Academy of Sciences, Chernogolovka, Moscow oblast, Russia*

**e-mail: sanina@icp.ac.ru*

Received February 18, 2022; revised February 24, 2022; accepted February 25, 2022

Abstract—Four compounds are synthesized by the reactions of rare-earth metal(III) nitrates with 2-mercaptopyridine-*N*-oxide (HSC_5H_4NO) in water-alkaline solutions: $[Pr_2(SC_5H_4NO)_6(H_2O)_2]$ (**I**), $[Tb_2(SC_5H_4NO)_6(H_2O)_2]$ (**II**), $[Ho_2(SC_5H_4NO)_6(H_2O)_2]$ (**III**), and $[Er_2(SC_5H_4NO)_6(H_2O)_2]$ (**IV**). Their synthesis and results of X-ray diffraction studies are presented. Each metal ion in the binuclear complexes forms the octacoordinated structure including two SC_5H_4NO ligands, which coordinate each metal ion (3+) via the chelate mode (through S and O), two bridging oxygen atoms belonging to two SC_5H_4NO, and two molecules of coordination water. The product χT and effective magnetic moment (μ_{eff}) remain unchanged in the synthesized complexes in the temperature range from 300 to 150 K as found by SQUID magnetometry. At $T <$ 150 K in complexes **I** ($T < 30$ K) and **II** ($T < 50$ K), μ_{eff} decreases with decreasing temperature, which possibly indicates a magnetic transition and an antiferromagnetic interaction between the Pr^{3+} and Tb^{3+} ions. An increase in μ_{eff} with decreasing temperature and a sharp decrease at $T < 10$ K are observed in complex **III**, whereas in complex **IV** μ_{eff} increases smoothly with decreasing temperature. This can indicate the appearance of ferromagnetic correlations in complex **IV**. No magnetic relaxation response is observed for complex **I** in the whole frequency range of the alternating field (AC) H_{AC} from 0.2 to 1400 Hz both in the bias field and without it. The field dependences of the magnetic moment at 2 and 5 K для complexes **II**–**IV** are characteristic of paramagnetics at these temperatures. At $T = 2$ K the samples exist in the same spin state as at $T = 300$ K: cooling does not change the spin state of the Tb^{3+}, Ho^{3+}, and Er^{3+} ions in the complexes. No magnetic hysteresis is observed at low temperatures (2 and 5 K) in these complexes. The dependences of the real and imaginary components of the magnetic susceptibility on the AC frequency for complexes **II**–**IV** are obtained in the absence of a direct field (DC) and in the bias field. The Cole-Cole diagrams demonstrate the relaxation mode of the domain wall motion and no shift of a maximum of the imaginary component with changing temperature (tunneling relaxation mechanism) in complexes **II**–**IV.**

Keywords: rare-earth metal complexes, 2-mercaptopyridine-*N*-oxide, X-ray diffraction, IR spectroscopy, SQUID magnetometry

DOI: 10.1134/S1070328422070089

INTRODUCTION

The design of new magnetics and establishment of structure–property relationships followed by the optimization of the properties of promising compounds and the production of related newest functional materials are urgent trends in the area of the modern materials science associated with permanently increasing demands of diminishing the electronic base of computing devices, increasing data recording density, and others. These materials can form a basis for the development of molecular spintronics and quantum computing [1]. The production of molecular nanomagnets with high temperatures of magnetization blocking can result in technological breakthroughs in the field of information technologies. An idea to use spins of electrons for data storage and processing is significant practical interest due to possible applications of the obtained molecular systems in molecular spintronics (spin switchers, molecular analogs of multiferroics, etc.) and quantum computations (molecular quantum cellular automata). Progress in the area of molecular magnetism and the recent (in 2010) discovery of monoionic magnetism make a substantial contribu-

tion to the development of this trend. The design of molecular nanomagnets based on the 3*d*- and 4*f*-metal complexes with the organic ligands, which demonstrate unusual magnetic properties within one molecule or one molecular chain at helium temperatures [2], is of special interest.

Lanthanide ions are good candidates for the development of single-molecule magnets (SMM), which is mainly caused by their significant magnetic anisotropy appeared for their high unquenched orbital angular moment. The lanthanide-based SMM demonstrate superiority in magnetism compared to other compounds, especially those containing Gd^{3+}, Tb^{3+}, and Dy^{3+} ions [3]. The dysprosium(III) and terbium(III) phthalocyanine complexes $[DyPc_2](TBA)$ and $[TbPc_2](TBA)$ (TBA = tetrabutylammonium, and Pc = phthalocyanine) were the first SMM containing lanthanide ions [4]. The whole series of SMM based on lanthanides has been synthesized to the present time [5–14], and the majority of them are presented by the Dy(III) complexes [15–24].

β-Diketones [25], nitronyl nitroxyl ligands of the imidazole series [26–31], and complexes with pyridine alcohols ($Py_n(CH_2)_m(OH)_k$ ($n = 1.2$; $m = 1.2$; $k = 0, 1, 2$)) [32] along with such ligands as polyoxometallates, phthalocyanines, and Schiff bases are used for the synthesis of these SMM.

The complexes based on rare-earth elements (REE) and 2-mercaptopyridine-*N*-oxide (HSC_5H_4NO) as the ligand are of interest for the design of new SMM and related materials [24]. Their structures and magnetic properties almost were not described in the literature. One of few examples is the description of the structure of the mononuclear samarium complex $Sm(HSC_5H_4NO)_3(DMSO)_2$ (DMSO = dimethyl sulfoxide) in which the solvent enters the composition of the complex, but the magnetic properties of this compound were not studied [33]. Similar mononuclear complexes based on praseodymium [34] and dysprosium [35] were synthesized later. More examples can be met among the "nonmagnetic" metals: the structures of the tin [36], bismuth [37], platinum [38], nickel [39], zinc [40], and copper [41] complexes were described.

The binuclear rare-earth metal (Pr(III), Tb(III), Ho(III), and Er(III)) complexes with mercaptopyridine-*N*-oxide (HSC_5H_4NO) were synthesized for the first time in this work. The influence of the nitroxyl-containing fragment on the structure formation of the complexes in aqueous solutions and magnetic characteristics was studied using X-ray diffraction, IR spectroscopy, and SQUID (Superconducting Quantum Interference Device) magnetometry.

EXPERIMENTAL

All reagents used in the work were commercial (Aldrich) and used as received (KOH and $Ho(NO)_3{\cdot}5H_2O$, $Pr(NO)_3{\cdot}6H_2O$, $Tb(NO)_3{\cdot}6H_2O$, $Er(NO)_3{\cdot}5H_2O$, and ligand $HSC_5H_4NO{\cdot}H_2O$). Bidistilled water was used to prepare solutions.

Synthesis of complexes I–IV (general procedure). A dry weighed sample of $HSC_5H_4NO{\cdot}H_2O$ (1.5 mmol, 0.0191 g) was added to KOH (1.5 mmol, 0.0846 g) dissolved in water (10 mL), and the mixture was vigorously stirred to obtain a transparent yellow solution. Then water (40 mL) and a prepared solution of the corresponding metal nitrate $M(NO)_3{\cdot}nH_2O$ (0.5 mmol, 0.2270 g) in water (50 mL) were added to the resulting solution. This reaction mixture was stirred for several minutes and left to stay for a week. The reaction products were single-phase, which is indicated by the data of elemental analysis and IR spectroscopy. The formed crystals of the complexes were filtered off and dried in air for 24 h. The yields were 74–78%. The general scheme of the synthesis of complexes **I–IV** is shown in Scheme 1.

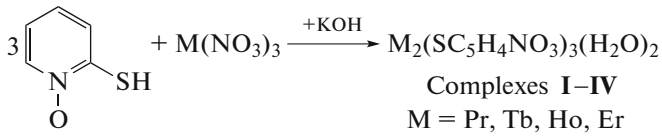

Scheme 1.

Analyses to C, H, N, S, and O in the complexes were carried out on a Vario El cube CHNS/O elemental analyzer at the Analytical Center of the Institute of Problems of Chemical Physics (Russian Academy of Sciences).

For $C_{30}H_{28}N_6O_8S_6Pr_2$ (**I**)

Anal. calcd., %	C, 33.55	H, 2.61	N, 7.82	O, 11.90	S, 17.90
Found, %	C, 33.53	H, 2.63	N, 7.80	O, 11.92	S, 17.89

For $C_{30}H_{28}N_6O_8S_6Tb_2$ (**II**)

Anal. calcd., %	C, 32.44	H, 2.53	N, 7.57	O, 11.52	S, 17.32
Found, %	C, 32.40	H, 2.55	N, 7.55	O, 11.50	S, 17.30

For $C_{30}H_{28}N_6O_8S_6Ho_2$ (**III**)

Anal. calcd., %	C, 32.09	H, 2.51	N, 7.48	O, 11.41	S, 17.13
Found, %	C, 32.10	H, 2.52	N, 7.50	O, 11.40	S, 17.10

For $C_{30}H_{28}N_6O_8S_6Ho_2$ (**IV**)

Anal. calcd., %	C, 31.96	H, 2.51	N, 7.45	O, 11.35	S, 17.06
Found, %	C, 32.00	H, 2.50	N, 7.43	O, 11.36	S, 17.04

The IR spectra of complexes **I**–**IV** were recorded on a Bruker ALPHA FT-IR spectrometer in a frequency range of 400–4000 cm^{-1} in the attenuated total reflection (ATR) mode.

IR for **I** (ν, cm^{-1}): 3199 w, 2192 vw, 1592 m, 1537 m, 1452 vs, 1413 vs, 1214 vs, 1191 vs, 1156 vs, 1139 vs, 1032 m, 978 w, 838 s, 822 s, 752 s, 701 s, 594 s, 579 s, 542 vs, 469 vs.

IR for **II** (ν, cm^{-1}): 3104 vw, 1594 vw, 1537.2 vw, 1450 m, 1401 vw, 1259 vw, 1215.8 m, 1186 vw, 1131 vw, 1073 vw, 1027 vw, 838 vw, 823.7 vw, 763 m, 752,3 m, 709 m, 596.2 m, 576 vw, 547 m.

IR for **III** (ν, cm^{-1}): 3609 vw, 3047 vw, 3022 vw, 1595 m, 1535 m, 1454 vs, 1413 vs, 1267 m, 1199 vs, 1148 vs, 1089 vs, 1032 m, 827 vs, 767 s, 746 vs, 707 s, 592 s, 551 s, 541 vs, 451 vs.

IR for **IV** (ν, cm^{-1}): 3046 vw, 1596 m, 1533 m, 1454 vs, 1414 m, 1267 m, 1199 vs, 1158 vs, 1149 vs, 1090 vs, 1033 m, 827 m, 770 m, 746 s, 708 s, 592 s, 553 s, 521 s, 452 s, 421 m, 405 m.

X-ray diffraction (XRD) of compounds **I**–**IV** was carried out on an Agilent XCalibur single-crystal diffractometer with an EOS detector (AgilentTechnologies UK Ltd., Yarnton, Oxfordshire, England). Data were collected and processed and unit cell parameters were determined and refined using the CrysAlis PRO program [42]. The structures were solved by a direct method. The positions and temperature parameters of non-hydrogen atoms were refined in the isotropic and then anisotropic approximations by full-matrix least squares. The positions of the hydrogen atoms in the anion were revealed from difference syntheses and refined by the riding model. The positions of the hydrogen atoms of the water molecule were revealed from the difference Fourier syntheses and refined with restraints imposed on bond lengths and thermal parameters.

All calculations were performed using the SHELXTL software [43]. The unit cell parameters and selected crystallographic data for complexes **I**–**IV** are given in Table 1.

The single-crystal XRD data for the structures of compounds **I**–**IV** were deposited with the Cambridge Crystallographic Data Centre (CIF files CCDC nos. 2143309–2143312; deposit@ccdc.cam.ac.uk, http://www.ccdc.cam.ac.uk).

SQUID magnetometry. Magnetic measurements were carried out using an MPMS 5XL Quantum design magnetometer. The temperature dependence of the magnetic susceptibility (χ(*T*)) was measured in a temperature range of 2–300 K at the DC magnetic field intensity H_{DC} = 1 kOe. The field dependence of the magnetization was measured at temperatures of 2 and 5 K. The frequency dependences of the real *m*' and imaginary *m*'' components of the magnetic susceptibility (χ) in an AC magnetic field of 2 Oe were recorded in a temperature range of 1.8–10 K. The AC magnetic field frequencies were 0.2–1400 Hz.

RESULTS AND DISCUSSION

Complexes **I**–**IV** were synthesized by the reactions of the corresponding rare-earth metal nitrate with ligand 2-mercaptopyridine-*N*-oxide (pyrithione) in aqueous aerobic solutions in the presence of KOH, unlike the work [39] where alcoholic solutions of rare-earth metal chlorides and NaOH were used. Pyrithione in protonic media exists as a pair of tautomers, the main form of which is 1-hydroxy-2(1*H*)-pyridinethione and another form is 2-mercaptopyridinethiol-*N*-oxide [44] (Scheme 2). Pyrithione (C_5H_5NOS) can easily be coordinated to the REE ions (3+) by two donor atoms (oxygen and sulfur), and the NO group of the thiol form of the ligand can also act as an individual magnetic center between the adjacent REE ions (3+).

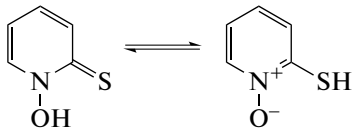

Scheme 2.

The coordination ability of 1-hydroxy-2-pyridinethione with various 3*d*-metal ions was well studied. The corresponding compounds were synthesized, and their spectral properties and magnetic susceptibility were investigated [45]. The complexes were found to form by chelation. The conjugated pyrithione base is the anion containing two donor atoms, sulfur atom, and oxygen atom, and each of them bears the formally negative charge. The nitrogen atom remains formally positively charged. The thiolate anion can be formed by the reaction with sodium carbonate, and pyrithionates are formed upon the addition of the metal(II) salt. The anion can act as the monodentate or bidentate ligand to form a complex with zinc(II) in the stoichiometric ligand to metal ratio equal to 1 : 2. Zinc pyrithione in the monomeric form has two anions chelated to zinc with the tetrahedral geometry. Zinc pyrithione in the solid state forms a dimer in which each zinc center adopts the trigonal bipyramidal geometry with two anions acting as lightening ligands coordinated via the oxygen atoms in the axial positions [46]. The thiolate anion coordinates as a bidentate ligand in the Mo clusters [47] and in the chromium(III) [48] or praseodymium(III) [34] complexes. In the case of a rare-earth metal, its coordination sphere has coordination sites occupied by solvent molecules, and they can be used in the design of new structures including SMM.

Compound **I** crystallizes in the monoclinic system. The crystal structure was refined in the space group $P2_1/n$, and its asymmetric moiety includes two Pr^{3+} ions, six $(SC_5H_4NO)^-$ anions, and two water molecules in the general position. The molecular structure

Table 1. Crystallographic data and experimental and structure refinement parameters for complexes **I**–**IV**

Parameters	Value			
	I	**II**	**III**	**IV**
Empirical formula	$C_{30}H_{28}N_6O_8S_6Pr_2$	$C_{30}H_{28}N_6O_8S_6Tb_2$	$C_{30}H_{28}N_6O_8S_6Ho_2$	$C_{30}H_{28}N_6O_8S_6Er_2$
FW	1074.76	1110.78	1122.80	1127.46
Temperature, K	150(1)	100(1)	150(1)	150.01(10)
Crystal size, mm	0.21 × 0.15 × 0.11	0.21 × 0.14 × 0.11	0.2 × 0.13 × 0.10	0.2 × 0.12 × 0.10
λ, Å	0.7107	0.7107	0.7107	0.7107
Crystal system	Monoclinic	Monoclinic	Monoclinic	Monoclinic
Space group	$P2_1/n$	$P2_1/c$	$P2_1/c$	$P2_1/c$
a, Å	19.6342(2)	9.99724(15)	9.9671(2)	9.9519(3)
b, Å	9.81100(10)	9.91810(16)	9.8900(2)	9.8585(3)
c, Å	20.2743(2)	19.1807(3)	19.1711(5)	19.1517(5)
α, deg	90	90	90	90
β, deg	94.1140(10)	94.4022(14)	94.392(2)	94.363(2)
γ, deg	90	90	90	90
V, Å^3	3895.40(7)	1896.23(5)	1884.23(7)	1873.56(9)
Z	4	2	2	2
ρ_{calc}, g/cm^3	1.833	1.945	1.979	1.999
μ, mm^{-1}	2.848	4.085	4.557	4.839
F(000)	2112	1080	1088	1092
Scan range over θ, deg	29.070	29.069	29.070	29.066
Measured reflections (R_{int})	22 923 (0.0206)	10 682 (0.0223)	1001 (0.0222)	10 017 (0.0265)
Independent reflections	10 411	5084	5051	5006
Number of refined parameters	481	241	241	241
R_1 ($I > 2\sigma(I)$)	0.0244	0.0222	0.0252	0.0301
wR_2 (for all data)	0.0524	0.0537	0.0545	0.0691
T_{min}/T_{max}	0.74639/1.00000	0.81502/1.00000	0.81999/1.00000	0.69106/1.00000
Residual electron density (ρ_{max}/ρ_{min}), e Å^{-3}	0.470/–0.766	0.540/–0.979	0.890/–1.154	1.090/–1.885

of complex **I** representing a binuclear complex is shown in Fig. 1. Each Pr^{3+} ion forms the octacoordinated (dodecahedral) structure including three $(SC_5H_4NO)^-$ ligands, which coordinate each Pr^{3+} ion via the chelate mode, bridging oxygen atoms O(3) and O(4) belonging to two $(SC_5H_4NO)^-$ ligands, and molecules of coordination water. Six single-charge anions $(SC_5H_4NO)^-$ fall onto two Pr^{3+} cations in the molecule, and the oxidation state of Pr is +3 according to the electroneutral conditions. The bond lengths and bond angles in binuclear complex **I** are given in Table 2. The corresponding bond lengths in each of eight coordination complexes are close, and some angles differ. For example, the chelate angles are equal in both complexes, whereas other angles differ noticeably because of the turns of the anions.

The shortened intermolecular contacts are observed in the structure of complex **I** (Table 3). The fragment of the crystal structure of complex **I** is shown in Fig. 2. It is seen from Fig. 2 that in the binuclear

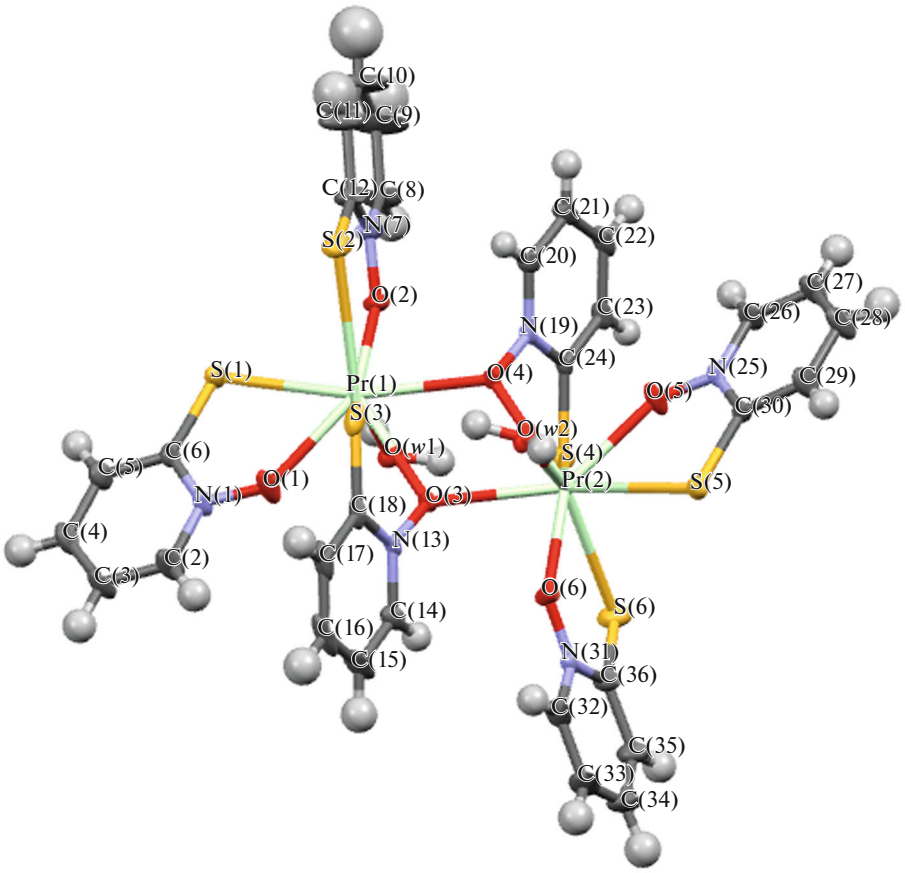

Fig. 1. Molecular structure of complex **I**. Atoms are presented as ellipsoids with 50% probability.

complex the fragments that could be bound by the inversion center participate in intermolecular contacts in different ways. The influence of these shortened contacts results in the distortion of the inversion center. In the crystal structure of complex **I**, the binuclear complexes join into pairs due to π-stacking interactions (C(32)...C(33) 3.384, C(32)...C(34) 3.291 Å). The distances between the metal atoms inside the molecules are 4.29 Å, and those between the adjacent atoms are 10.61 Å.

The crystal structure of complex **I** also contains both intra- and intermolecular hydrogen bonds (O(*w*)...S 3.10, 3.23 Å) (Fig. 3).

Compounds **II**–**IV** are completely isostructural and, hence, only the structure of the Ho(III) complex is described here.

Compound **III** crystallizes in the monoclinic system, and its asymmetric moiety contains the Ho^{3+} ion, three $(SC_5H_4NO)^-$ anions, and one water molecule in the general position. The molecular structure of complex **III** is shown in Fig. 4. The molecule represents the centrosymmetric binuclear complex. Each Ho^{3+} ion forms the octacoordinated structure including three 2-mercaptopyridine-*N*-oxide ligands, which chelate each Ho^{3+} ion via the chelate mode, bridging O(3) oxygen atom, and one molecule of coordination water. Six single-charge anions $(SC_5H_4NO)^-$ fall onto two Ho^{3+} cations, and the oxidation state of Ho is +3 according to the electroneutral conditions. The bond lengths and bond angles in binuclear complex **III** are listed in Table 4.

In the crystals of compounds **II**–**IV** (Fig. 5), the complexes are bound into three-dimensional structures due to weak van der Waals interactions unlike the crystals including the Pr(III) complexes (complex **I**). All three complexes exhibit intramolecular hydrogen bonds of the O(*w*)...S type (3.152 Å) (Fig. 6). However, the crystals of complex **I**, as mentioned previously, manifest similar hydrogen bonds between the adjacent complexes as well.

Thus, the crystal structure of compound **I** is stabilized due to hydrogen bonds and van der Waals interactions, whereas the crystal structures of compounds **II**–**IV** are stabilized only due to van der Waals interactions. Another feature of the crystal structure of compound **I** is that the pairs of binuclear complexes are formed due to π-stacking interactions.

The temperature dependence of the magnetic susceptibility $\chi(T)$ of complex **I** was recorded in the bias DC field at H_{DC} = 1000 Oe (inset in Fig. 7a). At the

Table 2. Bond lengths and angles in complex **I**

Bond	*d*, Å	Bond	*d*, Å
Pr(2)–O(5)	2.3625(17)	Pr(1)–O(1)	2.3638(18)
Pr(2)–O(6)	2.3665(16)	Pr(1)–O(2)	2.3487(16)
Pr(2)–O(*w*2)	2.4479(16)	Pr(1)–O(*w*1)	2.4797(17)
Pr(2)–O(4)	2.5087(15)	Pr(1)–O(3)	2.5129(15)
Pr(2)–O(3)	2.5302(15)	Pr(1)–O(4)	2.5103(15)
Pr(2)–S(6)	2.8742(7)	Pr(1)–S(2)	2.9253(7)
Pr(2)–S(5)	2.9801(6)	Pr(1)–S(1)	2.9445(6)
Pr(2)–S(4)	3.0015(6)	Pr(1)–S(3)	2.9938(6)
Angle	ω, deg	Angle	ω, deg
O(5)Pr(2)O(6)	140.62(6)	O(2)Pr(1)O(1)	136.78(6)
O(5)Pr(2)O(*w*2)	98.18(7)	O(1)Pr(1)O(*w*1)	89.34(7)
O(6)Pr(2)O(*w*2)	78.37(6)	O(2)Pr(1)O(*w*1)	72.31(6)
O(5)Pr(2)O(4)	77.02(6)	O(1)Pr(1)O(3)	74.82(6)
O(6)Pr(2)O(4)	138.67(5)	O(2)Pr(1)O(3)	134.65(5)
O(*w*2)Pr(2)O(4)	79.76(5)	O(*w*1)Pr(1)O(3)	78.16(5)
O(5)Pr(2)O(3)	140.11(6)	O(1)Pr(1)O(4)	138.08(6)
O(6)Pr(2)O(3)	77.74(5)	O(2)Pr(1)O(4)	78.33(5)
O(*w*2)Pr(2)O(3)	75.90(5)	O(*w*1)Pr(1)O(4)	80.63(5)
O(4)Pr(2)O(3)	63.09(5)	O(4)Pr(1)O(3)	63.31(5)
O(5)Pr(2)S(6)	104.31(5)	O(1)Pr(1)S(2)	122.12(6)
O(6)Pr(2)S(6)	66.54(4)	O(2)Pr(1)S(2)	66.17(4)
O(*w*2)Pr(2)S(6)	144.20(5)	O(*w*1)Pr(1)S(2)	138.45(4)
O(4)Pr(2)S(6)	132.10(4)	O(3)Pr(1)S(2)	132.38(4)
O(3)Pr(2)S(6)	102.25(4)	O(4)Pr(1)S(2)	89.70(4)
O(5)Pr(2)S(5)	63.46(4)	O(1)Pr(1)S(1)	64.05(4)
O(6)Pr(2)S(5)	78.06(4)	O(2)Pr(1)S(1)	74.72(4)
O(*w*2)Pr(2)S(5)	74.72(4)	O(*w*1)Pr(1)S(1)	82.38(4)
O(4)Pr(2)S(5)	128.34(4)	O(3)Pr(1)S(1)	134.39(4)
O(3)Pr(2)S(5)	144.99(4)	O(4)Pr(1)S(1)	151.46(4)
S(6)Pr(2)S(5)	90.79(2)	S(2)Pr(1)S(1)	87.965(19)
O(5)Pr(2)S(4)	71.86(4)	O(1)Pr(1)S(3)	74.21(5)
O(6)Pr(2)S(4)	132.09(4)	O(2)Pr(1)S(3)	141.76(4)
O(*w*2)Pr(2)S(4)	142.65(4)	O(*w*1)Pr(1)S(3)	140.96(4)
O(4)Pr(2)S(4)	63.00(4)	O(3)Pr(1)S(3)	63.55(4)
O(3)Pr(2)S(4)	89.01(4)	O(4)Pr(1)S(3)	88.40(4)
S(6)Pr(2)S(4)	71.920(18)	S(2)Pr(1)S(3)	78.20(2)
S(5)Pr(2)S(4)	125.988(17)	S(1)Pr(1)S(3)	118.824(18)

Table 3. Intermolecular contacts in complex **I**

Atom 1	Atom 2	Symmetry procedures 1	Symmetry procedures 2	*d*, Å
O(*w*2)	C(34)	*x*, *y*, *z*	*x*, –1 + *y*, *z*	3.208
S(3)	C(16)	*x*, *y*, *z*	1.5 – *x*, –1/2 + *y*, 1.5 – *z*	3.496
S(1)	O(*w*1)	*x*, *y*, *z*	1 – *x*, –*y*, 1 – *z*	3.309
S(5)	O(*w*2)	*x*, *y*, *z*	1 – *x*, –*y*, 2 – *z*	3.195
C(32)	C(33)	*x*, *y*, *z*	1 – *x*, 1 – *y*, 2 – *z*	3.384
C(32)	C(34)	*x*, *y*, *z*	1 – *x*, 1 – *y*, 2 – *z*	3.291

temperatures from 300 to 30 K, the effective magnetic moment ($\mu_{eff} = (8\chi T)^{1/2}$) is temperature independent (Fig. 7a), whereas at $T < 30$ K the effective moment decreases with decreasing temperature. The calculated value for REE ions in the paramagnetic state is determined by the equation

$$\mu_{eff} = g_J (2J(J+1))^{1/2},$$

where g_J is the Lande g factor, and J is the total moment of the ion. The parameters are as follows: $g_J = 4/5$; $J = 4$, $S = 1$, $L = 5$, ground state term $^3H_4$, and electronic configuration $4f^2$. For two noninteracting Pr^{3+} ions, the calculated value of the magnetic moment ($\mu_{eff} = 5.06\ \mu_B$) is close to the value obtained for complex **I** at room temperature: $\mu_{eff} = 5.05\ \mu_B$. A decrease in the effective magnetic moment at $T < 30$ K indicates the antiferromagnetic exchange interaction between the praseodymium ions. No magnetic hysteresis was observed at low temperatures (2 and 5 K) in complex **I** (Fig. 7b).

The dependences of the real and imaginary components on the AC field frequency were measured without bias DC field and in the DC magnetic field at $H_{DC} = 2500$ Oe (Figs. 8a and 8b, respectively). In both cases, no changes in the real component of the magnetic susceptibility were observed with a change in the AC field frequency. Since the imaginary component of the magnetic susceptibility was not higher than 1% of the real component (both in the bias field and without it), it can be concluded that there is no magnetic relaxation response in complex **I** in the frequency range from 0.2 to 1400 Hz.

The absence of a relaxation response of complex **I** can be explained by different environments of Pr^{3+} when all atoms exist in the dodecahedral environment but only complex **I** is noncentrosymmetric unlike complexes **II**–**IV**.

The temperature dependence of the magnetic susceptibility of complex **II** in the bias DC field ($H_{DC} = 1000$ Oe) is shown in Fig. 9a (inset). The effective moment μ_{eff} remains unchanged in the temperature

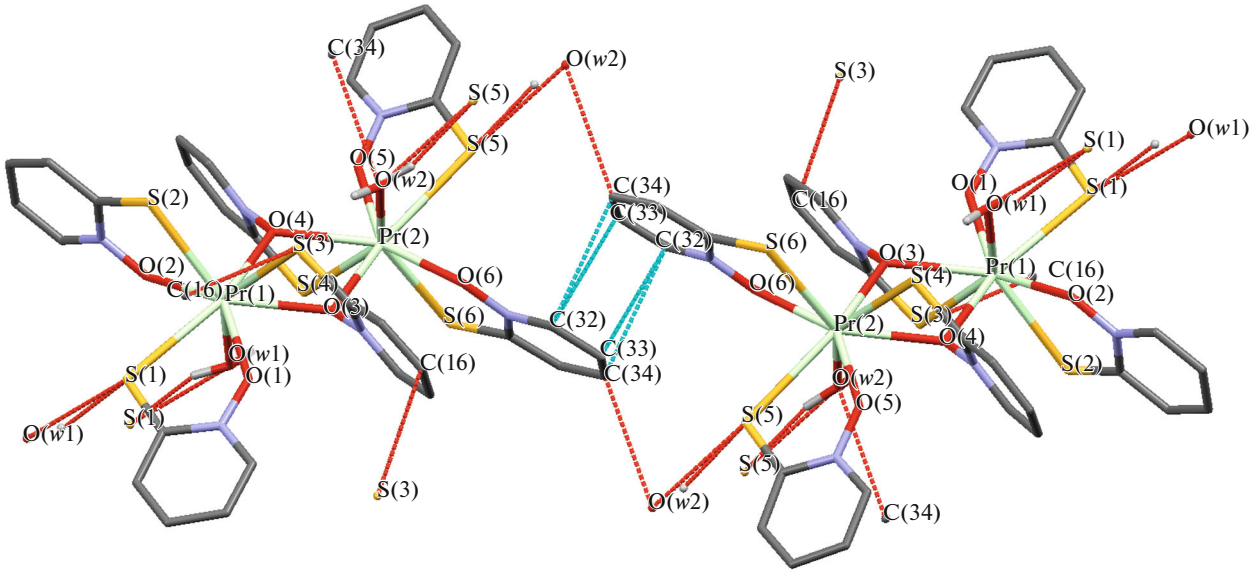

Fig. 2. Fragment of the crystal structure of complex **I**. Dashed lines show shortened intermolecular contacts.

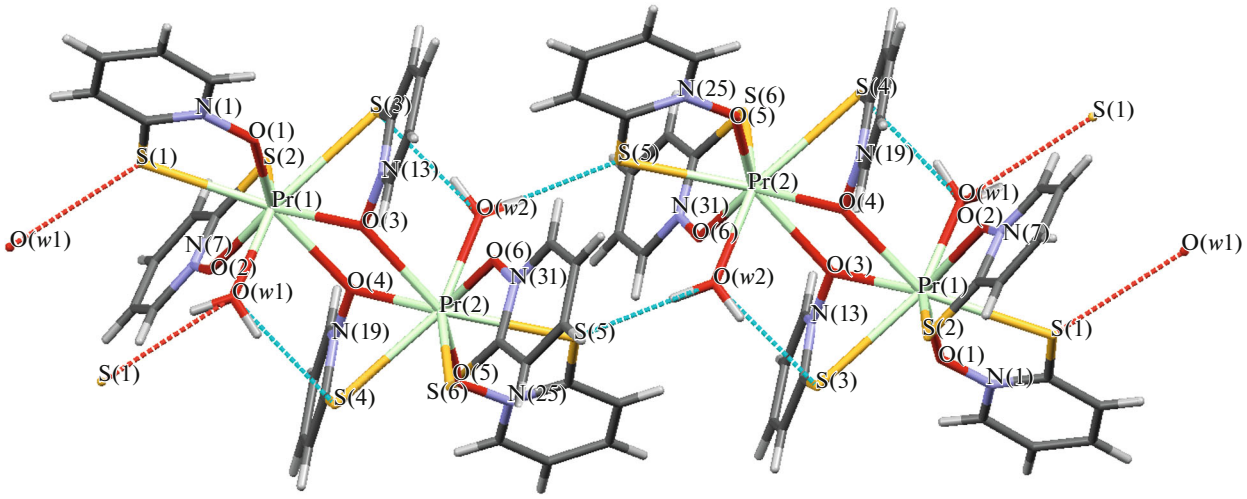

Fig. 3. Fragment of the crystal structure of complex **I**. Dashed lines show hydrogen bonds.

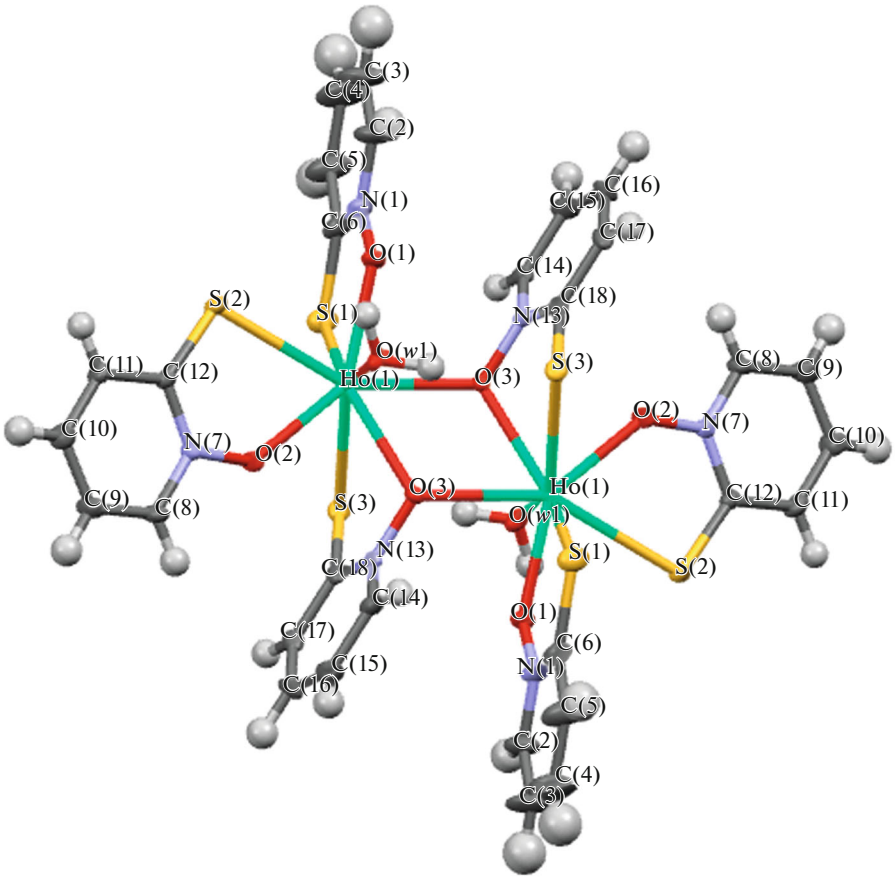

Fig. 4. Molecular structure of complex **III**. Atoms are presented as ellipsoids with 50% probability.

range from 300 to 50 K (Fig. 9a), and at $T < 50$ K μ_{eff} decreases with a temperature decrease. The parameters for the calculation of μ_{eff} of the Tb^{3+} ion are as follows: $g_J = 3/2$; $J = 6$, $S = 3$, $L = 3$, ground state term $^7F_6$, and electronic configuration $4f^8$. The calculated value for two Tb^{3+} ions ($\mu_{eff} = 13.70\ \mu_B$) is lower than the experimental value ($\mu_{eff} = 16.00\ \mu_B$). The experimental value of μ_{eff} can be described by the following

Table 4. Bond lengths and bond angles in complex **III**

Bond	*d*, Å	Bond	*d*, Å
Ho(1)–O(1)	2.257(2)	Ho(1)–S(1)	2.7906(8)
Ho(1)–O(2)	2.263(2)	Ho(1)–S(2)	2.8775(7)
Ho(1)–O(*w*1)	2.346(2)	Ho(1)–S(3)$^{\#1}$	2.9027(8)
Ho(1) –O(3)	2.4105(19)	S(2)–C(12)	1.705(3)
Ho(1)–O(3)$^{\#1}$	2.4145(19)	S(3)–C(18)	1.734(3)
Angle	ω, deg	Angle	ω, deg
O(1)Ho(1)O(2)	138.04(7)	O(3)$^{\#1}$Ho(1)S(1)	131.44(5)
O(1)Ho(1)O(*w*1)	75.53(7)	O(1)Ho(1)S(2)	72.35(5)
O(2)Ho(1)O(*w*1)	90.25(9)	O(2)Ho(1)S(2)	66.01(5)
O(1)Ho(1)O(3)	77.90(7)	O(*w*1)Ho(1)S(2)	77.33(5)
O(2)Ho(1)O(3)	140.17(7)	O(3)Ho(1)S(2)	147.50(5)
O(*w*1)Ho(1)O(3)	82.92(7)	O(3)$^{\#1}$Ho(1)S(2)	134.35(5)
O(1)Ho(1)O(3)$^{\#1}$	133.34(7)	S(1)Ho(1)S(2)	89.85(2)
O(2)Ho(1)O(3)$^{\#1}$	77.74(7)	O(1)Ho(1)S(3)$^{\#1}$	140.29(6)
O(*w*1)Ho(1)O(3)$^{\#1}$	76.00(7)	O(2)Ho(1)S(3)$^{\#1}$	72.46(6)
O(3)Ho(1)O(3)$^{\#1}$	62.52(8)	O(*w*1)Ho(1)S(3)$^{\#1}$	139.60(6)
O(1)Ho(1)S(1)	69.55(6)	O(3)Ho(1)S(3)$^{\#1}$	87.73(5)
O(2)Ho(1)S(1)	114.27(7)	O(3)$^{\#1}$Ho(1)S(3)$^{\#1}$	64.90(5)
O(*w*1)Ho(1)S(1)	145.00(6)	S(1)Ho(1)S(3)$^{\#1}$	74.20(2)
O(3)Ho(1)S(1)	91.84(5)	S(2)Ho(1)S(3)$^{\#1}$	123.77(2)

parameters: $g_J = 7/4$ (overestimated value) and $J = 6$. A decrease in μ_{eff} at the temperature lower than 50 K, as in the case of complex **I**, can indicate the antiferromagnetic interaction between the terbium ions. The shape of the field dependences of the magnetic moment of complex **II** at 2 and 5 K (Fig. 9b) is characteristic of a paramagnetic at the given temperatures. The dependences are described by the Brilloin function, but the spins, as it was expected, are higher than those for Tb^{3+} ions ($J = 6.7$ Hz). No magnetic hysteresis was observed at 2 and 5 K (Fig. 9b).

The frequency dependences of the real and imaginary components of the AC magnetic susceptibility of complex **II** in the absence of a magnetic field are shown in Fig. 10. The imaginary component of the magnetic susceptibility χ" vanishes at the temperature

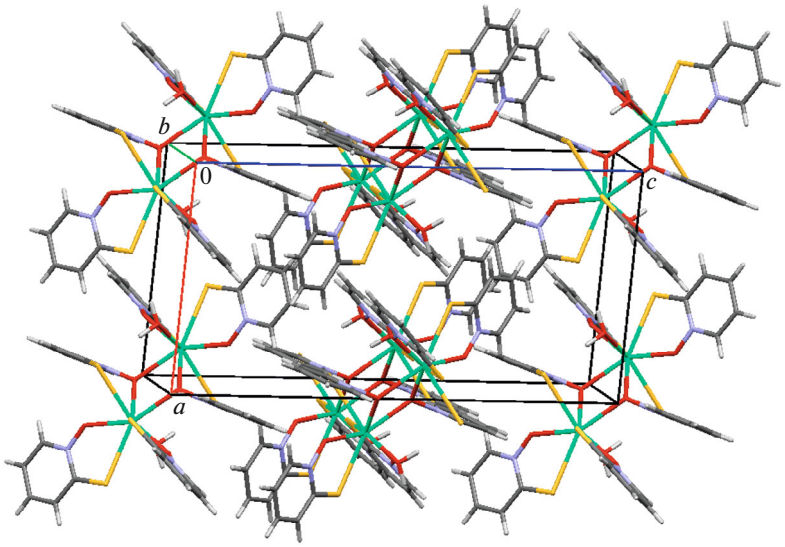

Fig. 5. Crystal packing of complex **III**.

higher than 3 K. In the temperature range from 1.8 to 3.0 K, the imaginary component of susceptibility χ" demonstrates a maximum at ~50 Hz, which is temperature-independent, indicating the zero activation energy obtained from the Arrhenius equation

$$f = f_0 \exp(-E_A/k_B T),$$

where E_A is the activation energy, and k_B is the Boltzmann constant. The Cole-Cole diagram at 1.8–3.0 K

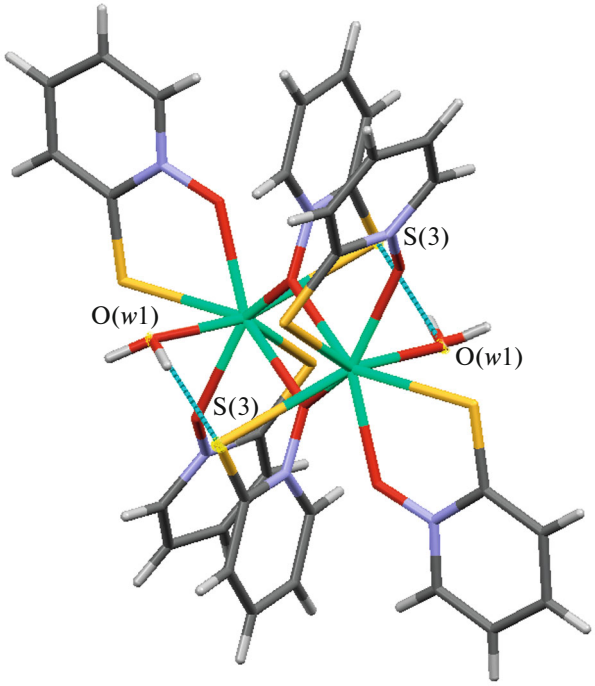

Fig. 6. Structures of binuclear complexes **II**–**IV**. Dashed lines show hydrogen bonds.

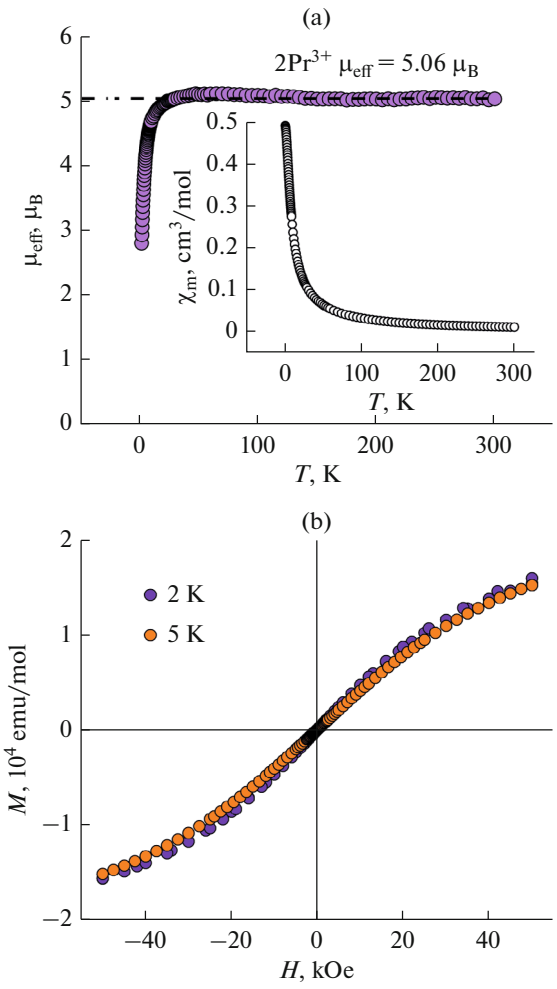

Fig. 7. Temperature dependences of the (inset) magnetic susceptibility and (a) effective magnetic moment of complex **I** (calculated μ_{eff} for two Pr^{3+} ions is shown by dotted lines) and (b) field dependences of the magnetic moment of complex **I** at temperatures of 2 and 5 K.

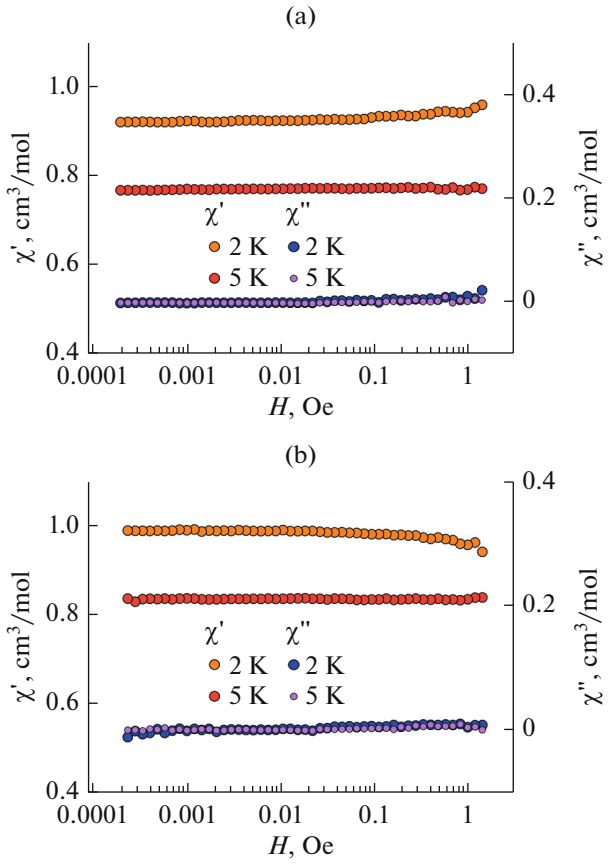

Fig. 8. Frequency dependences of the real and imaginary components of the magnetic susceptibility of complex **I** measured (a) without bias DC field and (b) in the bias field (H_{DC} = 2500 Oe).

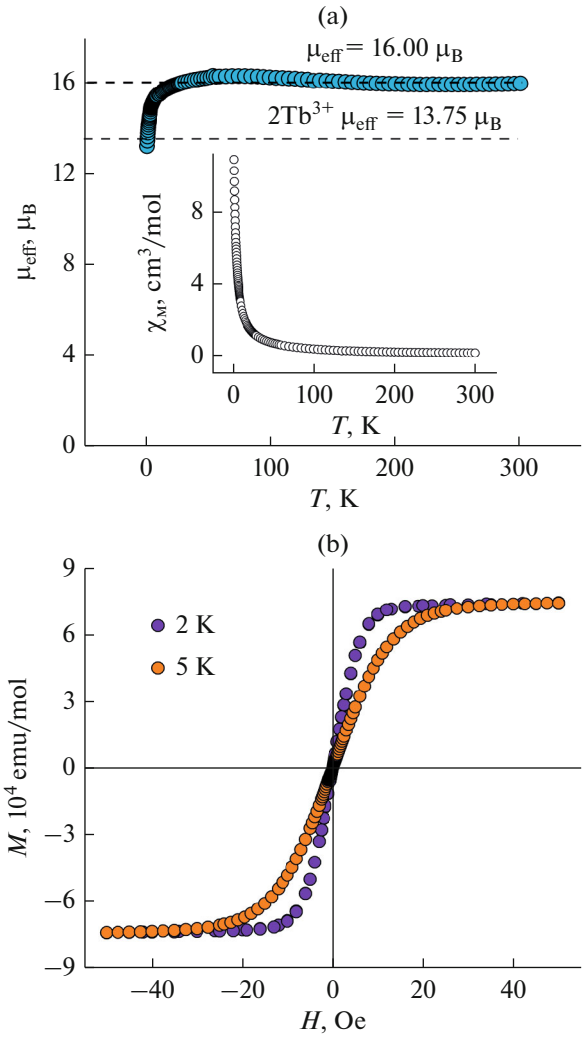

Fig. 9. Temperature dependences of the (inset) magnetic susceptibility and (a) effective magnetic moment of complex **II** (calculated μ_{eff} for two Tb^{3+} ions and an experimental value of 16.00 μ_B described in the text are shown by dotted lines) and (b) field dependences of the magnetic moment of complex **II** at temperatures of 2 and 5 K.

(Fig. 11) shows that the relaxation mode of the domain wall motion is observed in the sample [49]. In the case of zero activation energy, this can correspond to the tunneling relaxation mechanism [50].

The temperature dependence of the effective magnetic moment of complex **III** is shown in Fig. 12a. The effective moment remains unchanged at the temperatures from 300 to 150 K, and at $T < 150$ K μ_{eff} increases with a temperature decrease and decreases sharply at $T < 10$ K. The parameters for the calculation of the effective moment of the Ho^{3+} ion are as follows: $g_J = 5/4$; $J = 8$, $S = 2$, $L = 6$, ground state term $^5I_8$, and electronic configuration $4f^{10}$. The calculated value of μ_{eff} for two Ho^{3+} ions (15.00 μ_B) coincides with the experimental value obtained at room temperature (14.98 μ_B). An increase in the magnetic susceptibility at $T < 150$ K can indicate the appearance of ferromagnetic correlations in the sample at these temperatures, and the further decrease in the magnetic moment at $T < 10$ K corresponds to the antiferromagnetic interaction between the holmium ions at this temperature. The field dependences of the magnetic moment of complex **III** (Fig. 12b) are characteristic of a paramagnetic and described by the Brilloin function with the spin and g factor determined earlier from the temperature dependence of μ_{eff} at room temperature ($g_J = 5/4$; $J = 8$). Thus, at $T = 2$ K the sample exists in the same spin state as at $T = 300$ K (cooling does not change the spin state of the holmium ions in the complex). No magnetic hysteresis was observed at low temperatures (2 and 5 K) (Fig. 12b).

The field dependences of the real and imaginary components of the magnetic AC susceptibility for complex **III** at different temperatures and fields are shown in Fig. 13. At $T = 2$ K, the maximum of the imaginary component was observed at the same frequency (~50 Hz) in both cases.

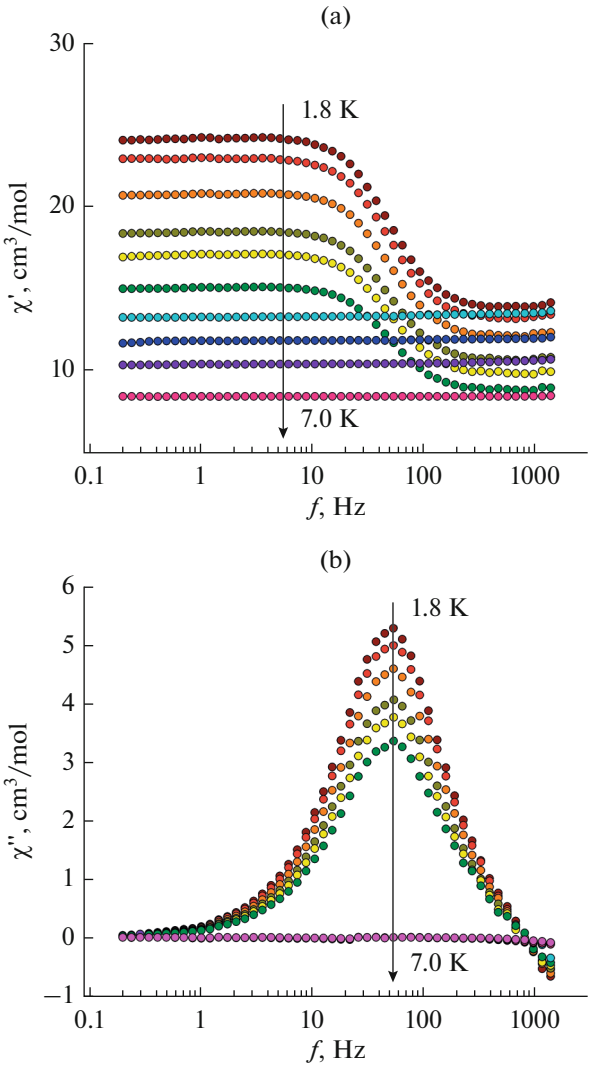

Fig. 10. Frequency dependences of the (a) real and (b) imaginary components of the magnetic susceptibility of complex **II** measured without bias DC field.

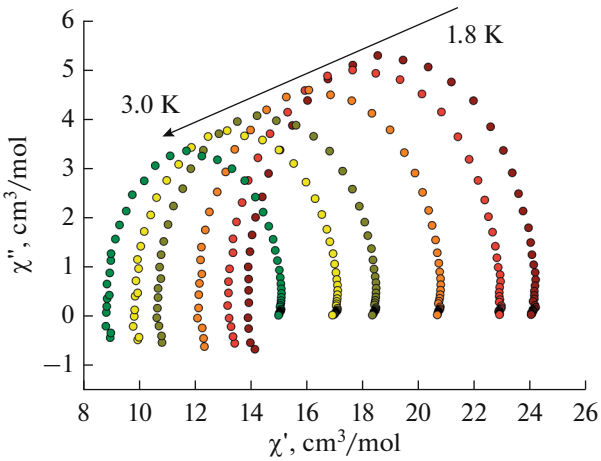

Fig. 11. Cole-Cole diagrams for the real and imaginary components of the magnetic susceptibility of complex **II** in the temperature range from 1.8 to 3.0 K. External DC field: $H_{DC} = 0$ Oe.

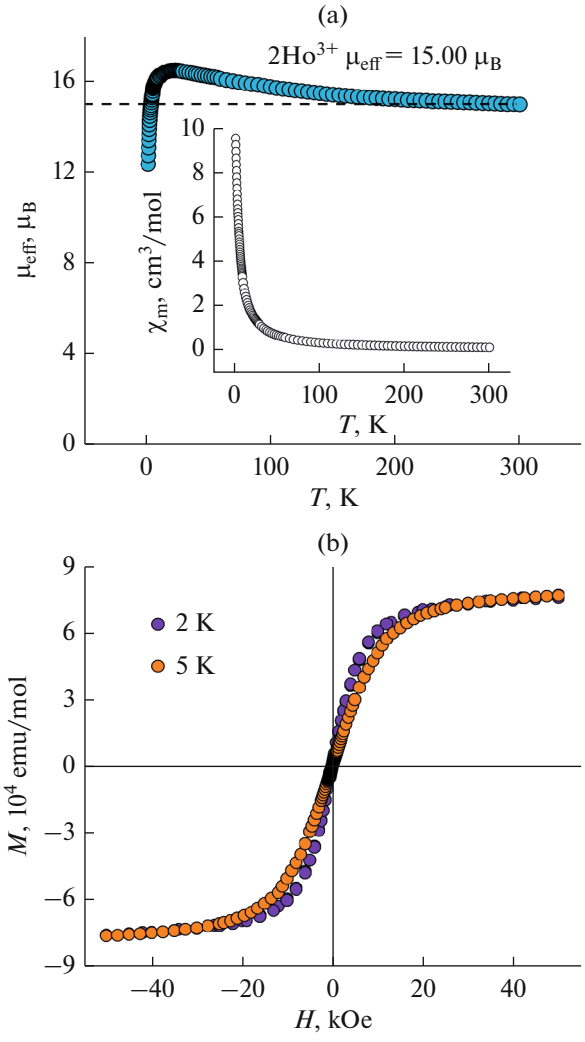

Fig. 12. Temperature dependences of the (inset) magnetic susceptibility and (a) effective magnetic moment of complex **II** (calculated μ_{eff} for two Ho^{3+} ions is shown by dotted lines) and (b) field dependences of the magnetic moment of complex **II** at temperatures of 2 and 5 K.

The temperature dependence of the effective magnetic moment of complex **IV** is shown in Fig. 14a. At the temperatures from 300 to 150 K, μ_{eff} does not change with a temperature change, and the effective moment increases at $T < 150$ K. The parameters for the calculation of the effective moment of the Er^{3+} ion are as follows: $g_J = 6/5$; $J = 15/2$, $S = 3/2$, $L = 6$, ground state term $^4I_{15/2}$, electronic configuration $4f^{11}$, and the calculated value of μ_{eff} for two Er^{3+} ions equal to 13.55 μ_B. The calculated value coincides with the experimental one at $T = 300$ K (13.32 μ_B). An increase in the magnetic susceptibility at $T < 150$ K can indicate the appearance of ferromagnetic correlations in the sample. The field dependences of the magnetic moment of complex **III** at temperatures of 2 and 5 K

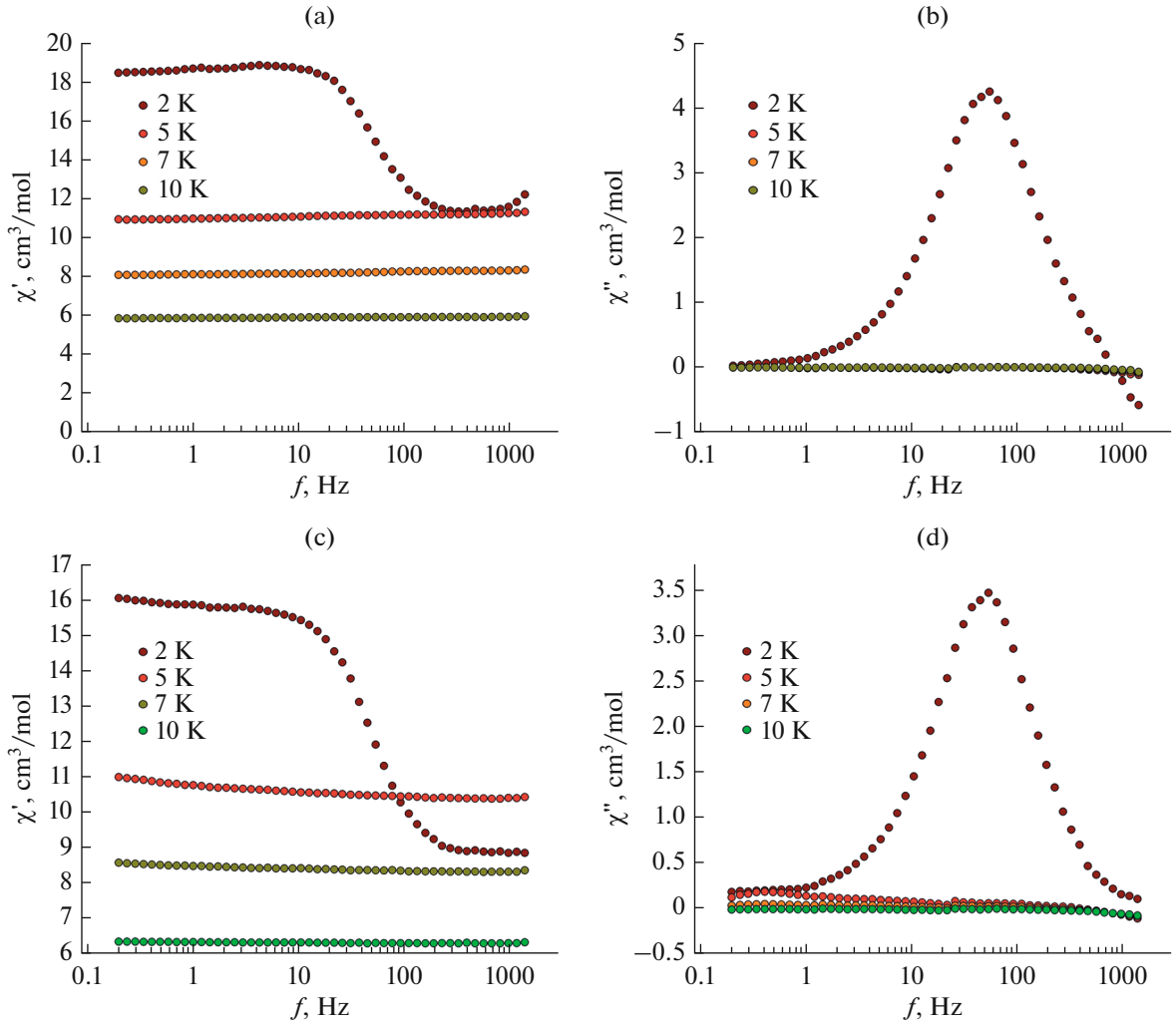

Fig. 13. Frequency dependences of the (a, c) real and (b, d) imaginary components of the magnetic susceptibility of complex **III** measured (a) without bias DC field and (b) in the bias field H_{DC} = 2500 Oe.

(Fig. 14b) have the shape characteristic of a paramagnetic and are described by the Brilloin function with the spin and *g* factor determined earlier from the temperature dependence of μ_{eff} at room temperature (g_J = 5/4; J = 8). Thus, cooling does not change the spin state of the erbium ions in the complex. No magnetic hysteresis was observed at low temperatures (2 and 5 K) as well (Fig. 14b).

The dependences of the real and imaginary components of the magnetic susceptibility on the AC field frequency without bias DC field are shown in Fig. 15 (Figs. 15a, 15b). The imaginary component of the magnetic susceptibility χ" vanishes at the temperature higher than 2.5 K, whereas in the temperature range from 2.0 to 2.5 K the imaginary component of susceptibility χ" demonstrates a temperature-independent maximum at a frequency of 50 Hz. The application of the external DC field (H_{DC} = 500 Oe was determined from the maximum of the field dependence of the imaginary component of the magnetic susceptibility) to the sample of complex **IV** does not change the frequency behavior of the real and imaginary components of the magnetic susceptibility (Figs. 15c, 15d). In both cases (without external field and in the presence of an external field), the imaginary component of susceptibility χ" demonstrates a temperature-independent maximum at a frequency of ~50 Hz, which is similar to the behavior of complex **II**.

The Cole-Cole diagram (Fig. 16) shows the relaxation mode of the domain wall motion and no shift of the maximum of the imaginary component with a temperature change as in the case of complex **II** (tunneling relaxation mechanism).

To conclude, it is found by XRD that the 2-mercaptopyridine-*N*-oxide ligand has several electron-donating centers in the complex formation with the

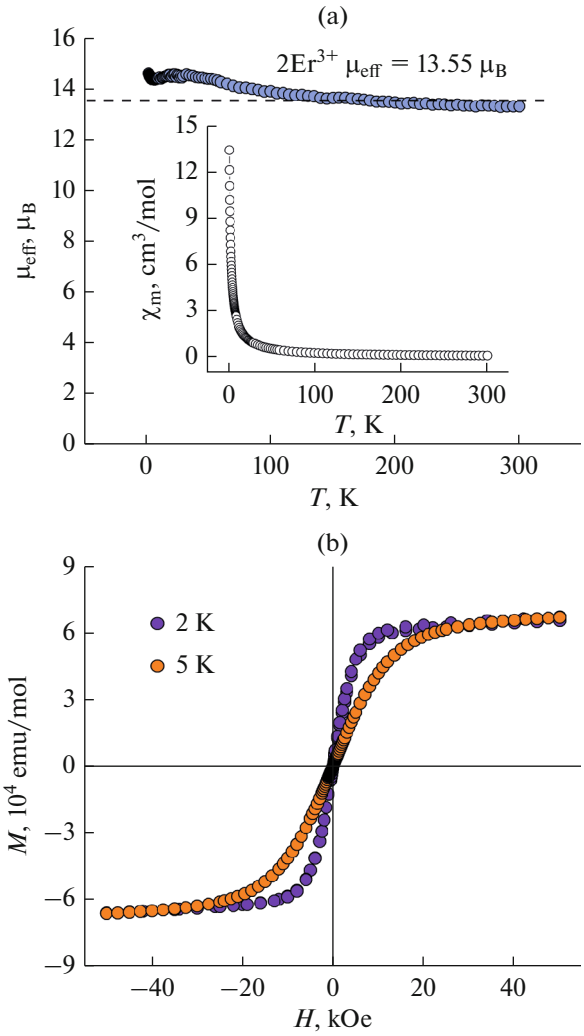

Fig. 14. Temperature dependences of the (inset) magnetic susceptibility and (a) effective magnetic moment of complex **II** (calculated μ_{eff} for two Er^{3+} ions is shown by dotted lines) and (b) field dependences of the magnetic moment of complex **II** at temperatures of 2 and 5 K.

rare-earth metals Pr(III), Tb(III), Ho(III), and Er(III) and manifests the bi- and tridentate properties to form binuclear complexes **I**–**IV** in an alkaline medium at the ligand to REE ratio equal to 3 : 1.

The XRD results showed that water molecules were involved in complex formation along with the oxygen and sulfur atoms of the ligand. The crystal structure of complex **I** also exhibit both intra- and intermolecular hydrogen bonds (O(*w*)...S). Only intramolecular hydrogen bonds (O(*w*)...S) are observed in complexes **II**–**IV**.

The magnetic properties of binuclear complexes **I**–**IV** were studied by SQUID magnetometry in a wide temperature range. Complexes **II**–**IV** demonstrate the magnetic behavior characteristic of complexes with rare-earth metals. The temperature dependences of the magnetic moment assume a significant magnetic anisotropy. The frequency dependences demonstrate a slow relaxation of magnetization and can be described by the generalized Debye model, and one relaxation time is used regardless of temperature. This behavior is characteristic of monomolecular magnets with the predomination of quantum tunneling. This fact is confirmed by the absence of hysteresis effects on the field dependences of the magnetic moment.

FUNDING

This work was supported by the Ministry of Education and Science of the Russian Federation (state assignment AAAA-A19-119092390079-8).

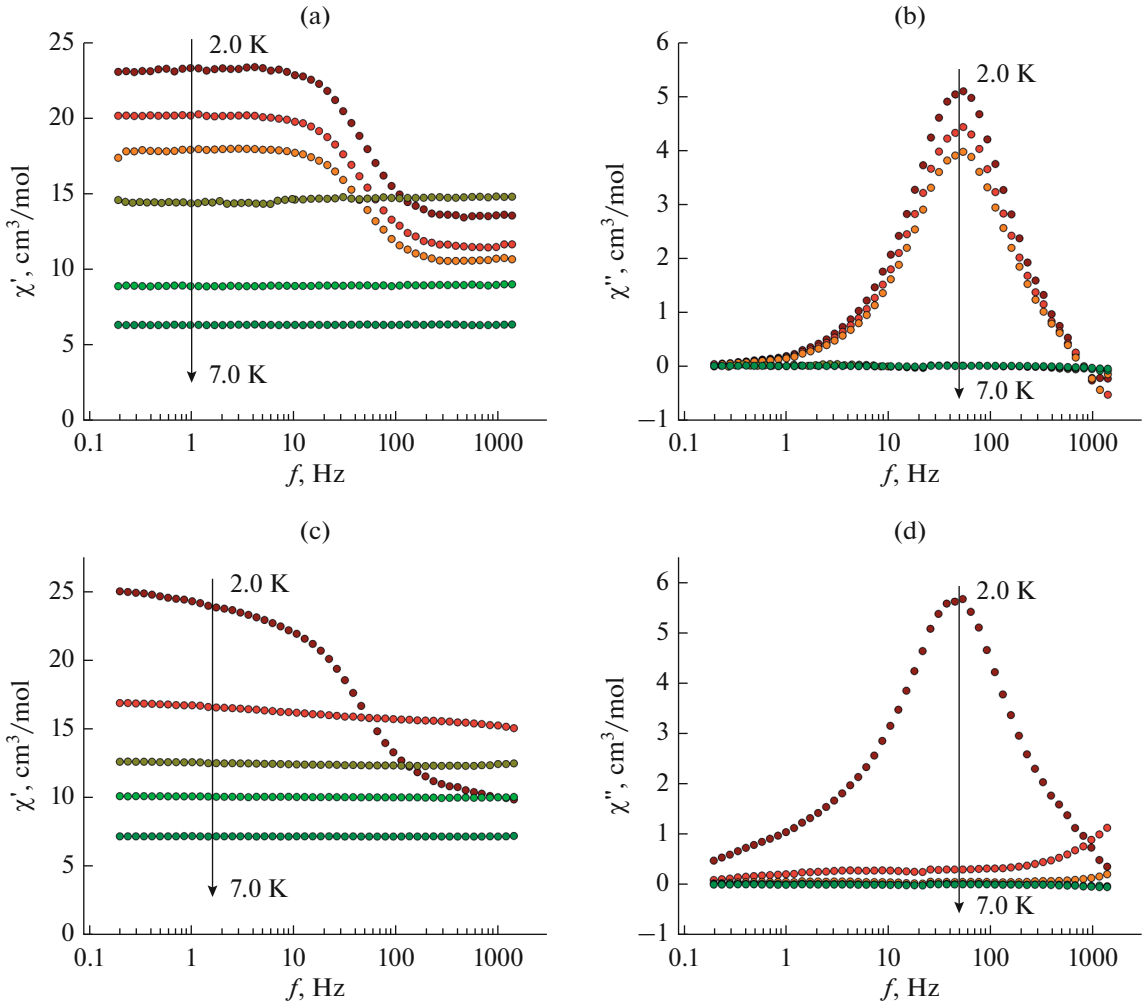

Fig. 15. Frequency dependences of the (a, c) real and (b, d) imaginary components of the magnetic susceptibility of complex **IV** measured (a) without bias DC field and (b) in the bias field H_{DC} = 500 Oe.

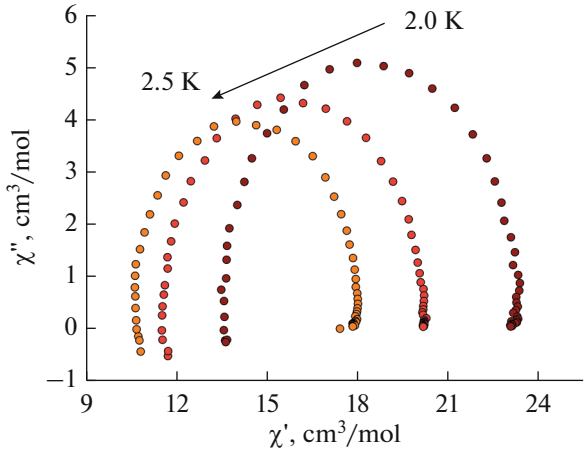

Fig. 16. Cole-Cole diagrams for the imaginary and real components of the magnetic susceptibility of complex **IV** at 2.00, 2.25, and 2.50 K. External DC field: H_{DC} = 500 Oe.

CONFLICT OF INTEREST

The authors declare that they have no conflicts of interest.

REFERENCES

1. Montgomery, C.P. and Murray, B.S., New, E.J., et al., *Acc. Shem. Res.*, 2009, vol. 42, no. 7, p. 925.
2. Stamatatos, T.C., Teat, S.J., Wernsdorfer, W., et al., *Angew. Chem., Int. Ed. Engl.*, 2009, vol. 48, no. 3, p. 521.
3. Kühne, I.A., Magnani, N., Mereacre, V., et al., *Chem. Commun.*, 2014, p. 1882.
4. Ishikawa, N., Sugita, M., Ishikawa, T., et al., *J. Am. Chem. Soc.*, 2003, vol. 125, no. 29, p. 8694.
5. Zhang, Y.Z., Duan, G.P., Sato, O., et al., *J. Mater. Chem.*, 2006, vol. 16, no. 26, p. 2625.
6. Gao, S., Su, G., Yi, T., et al., *Phys. Rev. B*, 2001, vol. 63, no. 5, p. 054431.

7. Sugita, M., Ishikawa, N., Ishikawa, T., et al., *Inorg. Chem.*, 2006, vol. 45, no. 3, p. 1299.

8. Benelli, C. and Gatteschi, D., *Chem. Rev.*, 2002, vol. 102, no. 6, p. 2369.

9. Ishikawa, N., Sugita, M., Ishikawa, T., et al., *J. Am. Chem. Soc.*, 2003, vol. 125, no. 29, p. 8694.

10. Ishikawa, N., Sugita, M., Ishikawa, T., et al., *J. Phys. Chem. B*, 2004, vol. 108, no. 31, p. 11265.

11. Ishikawa, N., Sugita, M., and Wernsdorfer, W., *Angew. Chem., Int. Ed. Engl.*, 2005, vol. 44, no. 19, p. 2931.

12. Ishikawa, N., Sugita, M., and Wernsdorfer, W., *J. Am. Chem. Soc.*, 2005, vol. 127, no. 11, p. 3650.

13. AlDamen, M.A., Clemente-Juan, J.M., Coronado, E., et al., *J. Am. Chem. Soc.*, 2008, vol. 130, no. 28, p. 8874.

14. AlDamen, M.A., Cardona-Serra, S., Clemente-Juan, J.M., et al., *Inorg. Chem.*, 2009, vol. 48, no. 8, p. 3467.

15. Layfield, R.A., McDouall, J.J., Sulway, S.A., et al., *Chem.-Eur. J.*, 2010, vol. 16, no. 15, p. 4442.

16. Tang, J., Hewitt, I., Madhu, N., et al., *Angew. Chem.*, 2006, vol. 118, no. 11, p. 1761.

17. Zheng, Y.Z., Lan, Y., Anson, C.E., et al., *Inorg. Chem.*, 2008, vol. 47, no. 23, p. 10813.

18. Gamer, M.T., Lan, Y., Roesky, P.W., et al., *Inorg. Chem.*, 2008, vol. 47, no. 15, p. 6581.

19. Wang, Y., Li, X.L., Wang, T.W., et al., *Inorg. Chem.*, 2010, vol. 49, no. 3, p. 969.

20. Sessoli, R. and Powell, A.K., *Coord. Chem. Rev.*, 2009, vol. 253, nos. 19–20, p. 2328.

21. Jiang, S.D., Wang, B.W., Su, G., et al., *Angew. Chem.*, 2010, vol. 122, no. 41, p. 7610.

22. Guettas, D., Gendron, F., Fernandez Garcia, G., et al., *Chem.-Eur. J.*, 2020, vol. 26, no. 19, p. 4389.

23. Yi, X., Bernot, K., Pointillart, F., et al., *Chem.-Eur. J.*, 2012, vol. 18, no. 36, p. 11379.

24. Yi, X., Pointillart, F., Le Guennic, B., et al., *Polyhedron*, 2019, vol. 164, p. 41.

25. Wang, W.M., Zhang, H.X., Wang, S.Y., et al., *Inorg. Chem.*, 2015, vol. 54, no. 22, p. 10610.

26. Bernot, K., Luzon, J., Bogani, L., et al., *J. Am. Chem. Soc.*, 2009, vol. 131, no. 15, p. 5573.

27. Zhou, N., Ma, Y., Wang, C., et al., *Dalton Trans.*, 2009, no. 40, p. 8489.

28. Bernot, K., Pointillart, F., Rosa, P., et al., *Chem. Commun.*, 2010, vol. 46, no. 35, p. 6458.

29. Wang, X.L., Li, L.C., and Liao, D.Z., *Inorg. Chem.*, 2010, vol. 49, no. 11, p. 4735.

30. Mei, X.L., Ma, Y., Li, L.C., et al., *Dalton Trans.*, 2012, vol. 41, no. 2, p. 505.

31. Liu, R.N., Zhang, C.M., Li, L.C., et al., *Dalton Trans.*, 2012, vol. 41, no. 39, p. 12139.

32. Bao, D.X., Xiang, S., Wang, J., et al., *J. Coord. Chem.*, 2016, vol. 69, no. 21, p. 3131.

33. Xiong, R.G., Zuo, J.L., You, X.Z., et al., *Polyhedron*, 1996, vol. 15, no. 19, p. 3321.

34. Niu, D.Z., Mu, L.L., Lu, Z.S., et al., *J. Chem. Crystallogr.*, 2004, vol. 34, no. 3, p. 195.

35. Niu, D.Z. and Chen, J.T., *Chin. J. Struct. Chem.*, 2002, vol. 21, no. 5, p. 520.

36. Karwasara, S., Jha, C.K., Sinhababu, S., et al., *Dalton Trans.*, 2016, vol. 45, no. 17, p. 7200.

37. Niu, D.Z., Mu, L.L., Yu, S.Z., et al., *J. Chem. Crystallogr.*, 2003, vol. 33, no. 1, p. 27.

38. Ravindran Durai Nayagam, B., Jebas, S.R., and Schollmeyer, D., *Acta Crystallogr., Sect. E: Struct. Rep. Online*, 2008, vol. 64, no. 2, p. m425.

39. Chen, X., Hu, Y., Wu, D., et al., *Polyhedron*, 1991, vol. 10, nos. 23–24, p. 2651.

40. Liu, R., Liu, S., and Zhu, H., *J. Nanjing Univ. Technol. (Nat. Sci. Ed.)*, 2007, vol. 12, no. 3, p. 48.

41. Niu, D.Z., Yao, L., Min, X., et al., *Z. Kristallogr. New Cryst. Struct.*, 2011, vol. 226, no. 4, p. 527.

42. *Agilent CrysAlis PRO*, Agilent Technologies UK Ltd., Yarnton, Oxfordshire, England, 2011.

43. Sheldrick, G.M., *SHELXTL. Version 6.14. Structure Determination Software Suite*, Madison: Bruker AXS., 2000.

44. Bond, A. and Jones, W., *Acta Crystallogr., Sect. C: Cryst. Struct. Commun.*, 1999, vol. 55, no. 9, p. 1536.

45. Das, A., Han, Z., Brennessel, W.W., et al., *ACS Catal.*, 2015, vol. 5, no. 3, p. 1397.

46. Barnett, B.L., Kretschmar, H.C., and Hartman, F.A., *Inorg. Chem.*, 1977, vol. 16, no. 8, p. 1834.

47. Liang, H., Chen, Z.F., Hu, R.X., et al., *Transition Met. Chem.*, 2002, vol. 27, no. 1, p. 102.

48. Wen, T.B., Shi, J.C., Liu, Q.T., et al., *Acta Crystallogr., Sect. C: Cryst. Struct. Commun.*, 1996, vol. 52, no. 5, p. 1204.

49. Kleemann, W., *Annu. Rev. Mater. Res.*, 2007, vol. 37, p. 415.

50. Guo, Y.N., Xu, G.F., Guo, Y., et al., *Dalton Trans.*, 2011, vol. 40, no. 39, p. 9953.

Translated by E. Yablonskaya